Measurement of Number and Cross-sectional Area of Basal Cell Pseudopodia: A New Morphometric Method

TAKASHI OKAGAKI, BARBARA A. CLARK, and LEO B. TWIGGS
Departments of Obstetrics and Gynecology, and Laboratory Medicine and Pathology, University of Minnesota Medical School, Minneapolis, Minnesota 55455

ABSTRACT A method of morphometric quantitation of the number of pseudopodia per individual basal cell and the ratio of the total cross-sectional area of the pseudopodia to the base area of the basal cell, using the transmission electron microscope, was developed. The diameters and areas of the bases of basal cells and the pseudopodia were also obtained. The number of pseudopodia per basal cell ($\bar{N}$) and the ratio of the areas ($\bar{F}$) measured in normal human uterine cervical epithelium were 34.32 and 0.338, respectively. The values observed in reactive atypia were 23.62 and 0.188; and those in mild dysplasia of the cervical epithelium (the earliest premalignant condition of the cervical epithelium), 26.98 and 0.226. There were statistically significant reductions in the number of pseudopodia per cell ($\bar{N}$) and the ratio of areas ($\bar{F}$) in the latter two pathological conditions compared to the controls. This morphometric method provides a highly sensitive means by which one can quantify the characteristics of pseudopodia in various premalignant epithelia.

Recent observations have suggested that the interaction of stromal tissue with its associated epithelium might play a controlling role in epithelial tissue differentiation in carcinogenesis (1, 2, 4, 9). Some epithelial tissues, such as epidermis and uterine cervical epithelium, possess pseudopodia (Fig. 1). A basal lamina lines the interface and envelops the pseudopodia, forming outpouchings into the stroma. The functions of the pseudopodia are not well understood. They may mechanically strengthen the adherence between the epithelium and the stroma, or they may function to increase the surface area of this interface. Whatever the true function of the pseudopodia is, a reduced number of pseudopodia have been reported in malignant and premalignant epithelial lesions of the uterine cervix (10).

A section of the epithelial tissue viewed with the conventional transmission electron microscope fails to demonstrate the exact size and number of basal cell pseudopodia in the epithelium because the section plane is a two-dimensional representation and, thus, the total basal cell surface cannot be shown. We have developed a new stereologic method to quantify the total number of pseudopodia in each basal cell and to estimate the ratio of the cross-sectional area of the pseudopodia to that of the base of the basal cell.

Mathematical Models

Three assumptions can be made: first, a basal cell is a solid cylinder standing on a plane of basal lamina; second, the neck portion of a pseudopodium is a smaller cylinder (Fig. 2); third, a section plane is nearly vertical to the basal lamina observed by conventional transmission electron microscopy and intersects with the bases of the cylindrical cell and the pseudopodia. The height of the cylinder representing either a basal cell or a pseudopodium is irrelevant to the measurement of the cross-sectional areas in this model. From transmission electron micrographs, we measure the section planes intersecting the basal cell base and the corresponding intersects with the pseudopodia. With this measurement, using calculated expectancies of the intersects in terms of the radii, we are able to estimate the radii of the cylinders representing the basal cell and its pseudopodia. After this calculation, the areas of the cells and the pseudopodia can be known.

The first mathematical model will be based on the observation of more than one section plane made through a basal cell (multiple section—single cell model). This will be extended to a more realistic and practical calculation based on the observation of a section plane through each member of a sufficiently large number of basal cells (single section—multiple cell model). The mathematical symbols used are summarized in Appendix 1.

Multiple Section: Single Cell Model

First, the expectancy $\hat{L}_i$ of the ith cell is calculated using a variable t (Fig. 3) which is the distance of the intersect from

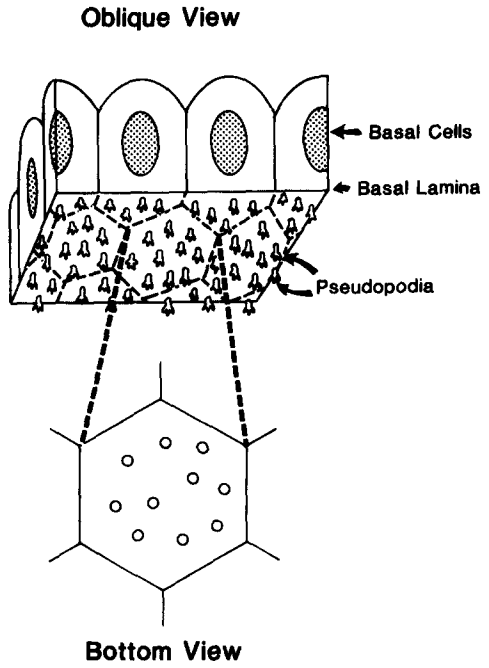

FIGURE 1 Schematic representation of pseudopodia extending into the stroma as seen from the stromal side of the basal cell-stromal interface.

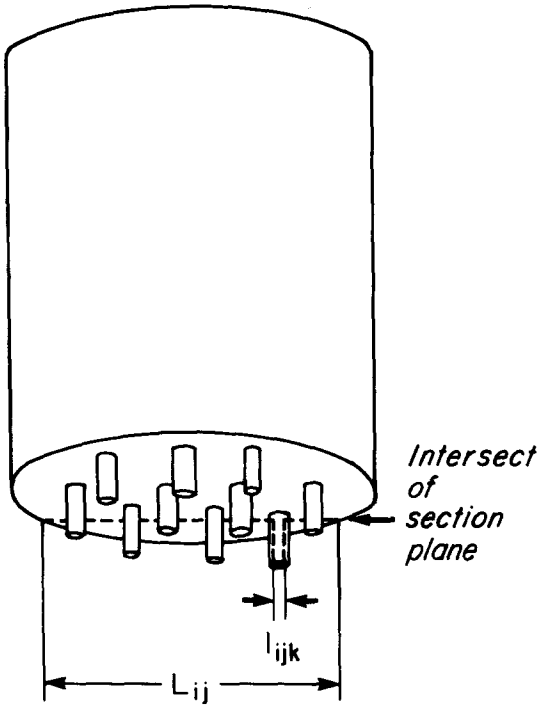

FIGURE 2 Stereological calculations of the base area of a basal cell and the basal area of a pseudopodium are based on the model assuming that they are cylinders with the radii $\hat{R}_i$ and $\hat{r}_i$. The lengths of the intersects of the jth plane with the base of the cell and the base of the pseudopodium are designated with L_{ij} and l_{ijk} respectively, where $i(= 1, \ldots, M)$, $j(= 1, \ldots m)$, and $k(= 1, \ldots, \hat{N}_i)$ represents the numerical designations of the cells, section planes, and pseudopodia.

the center of the circular base of the cell. That is

$$\hat{L}_i = \frac{\int_{-\hat{R}_i}^{\hat{R}_i} 2\sqrt{\hat{R}_i^2 - t^2} \cdot dt}{2\hat{R}_i} = \frac{\pi}{2}\hat{R}_i. \quad (1)$$

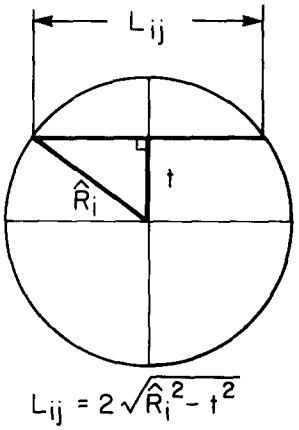

FIGURE 3 Schematic representation for calculation of expectancy of an intersect of the circular base of a basal cell.

One also sees that the population standard deviation of L_{ij} (the standard deviation of L_{ij} in an observation of infinite j),

$$\sigma_{\bar{L}_i} = \hat{R}_i \sqrt{\frac{8}{3} - \frac{\pi^2}{4}} \quad (2)$$

is approximately one-third of the magnitude of $\hat{L}_i$.
From Eq. 1,

$$\hat{A}_i = \frac{4}{\pi}\hat{L}_i^2. \quad (3)$$

Similarly, the expectancy of the length of the intersect between the base of the kth pseudopodium of the ith cell

$$\hat{l}_{ik} = \frac{\pi}{2}\hat{r}_{ik}. \quad (4)$$

Also

$$\hat{a}_{ik} = \frac{4}{\pi}\hat{l}_{ik}^2. \quad (5)$$

$\bar{L}_i$ and $\bar{l}_i$ obtained after observing a sufficiently large number of section planes m are the estimators of $\hat{L}_i$ and $\hat{l}_i$. From $\bar{L}_i$ and $\bar{l}_i$ one can obtain estimators of $\hat{R}_i$, $\hat{A}_i$, $\hat{r}_i$, and $\hat{a}_i$:

$$\bar{R}_i = \frac{2}{\pi}\bar{L}_i, \quad (6)$$

$$\bar{A}_i = \frac{4}{\pi}\bar{L}_i^2, \quad (7)$$

$$\bar{r}_i = \frac{2}{\pi}\bar{l}_i, \quad (8)$$

and

$$\bar{a}_i = \frac{4}{\pi}\bar{l}_i^2. \quad (9)$$

As defined, $\bar{N}_i$ is the number of pseudopodia in the ith cell from the observations of a finite number of sections, m. We defined $\bar{l}_{ij}$ such that

$$\bar{l}_{ij} = \frac{1}{n_{ij}} \cdot \sum_k^{n_{ij}} l_{ijk}, \quad (10)$$

whereas

$$\bar{n}_i = \frac{1}{m} \cdot \sum_j^{m} n_{ij}$$

converges to its expectancy $\hat{n}_i$ at a sufficiently large m.

From a simple calculation of a probability[1], one sees that

$$\frac{\hat{N}_i \cdot \hat{a}_i}{\hat{A}_i} = \frac{\hat{n}_i \cdot \hat{l}_i}{\hat{L}_i} = \hat{F}_i, \tag{11}$$

$$\text{or} \quad \hat{N}_i = \hat{n}_i \frac{\hat{L}_i}{\hat{l}_i}. \tag{12}$$

We define that

$$N_{ij} = n_{ij} \frac{\bar{L}_{ij}}{\bar{l}_{ij}}.$$

Let

$$N_{ij} = 0, \qquad \text{if } n_{ij} = 0.$$

Define $\bar{N}_i$ by:

$$\bar{N}_i = \frac{1}{m} \sum_j^m N_{ij}. \tag{13}$$

When the standard errors of $\bar{n}_i$, $\bar{L}_i$, and $\bar{l}_i$ are comparatively smaller than the magnitudes of $\bar{n}_i$, $\bar{L}_i$, and $\bar{l}_i$, $\bar{N}_i$ converges to $\hat{N}_i$ at a sufficiently large j.[2] That is, $\bar{N}_i$ is an estimator of $\hat{N}_i$.

The standard deviation is

$$\sqrt{\frac{\sum_j^m N_{ij}^2 - m\bar{N}_i^2}{m}},$$

and the standard error

$$\Delta\bar{N}_i = \frac{1}{m} \sqrt{\sum_j^m N_{ij}^2 - m\bar{N}_i^2}.$$

Similarly defining

$$\bar{F}_i = \frac{1}{m} \sum_j^m F_{ij},$$

where

$$F_{ij} = n_{ij} \frac{\bar{l}_{ij}}{\bar{L}_{ij}},$$

$\bar{F}_i$ is an estimator of the expectancy $\hat{F}_i$ in Eq. 11.

Single Section: Multiple Cell Model

The application of the multiple section—single cell method of the morphometry is a formidable task. In serial sections of a specimen, the identical cell or the identical pseudopodium in different section planes must be identified; and such identification is almost impossible. The multiple section—single cell model can be extrapolated to single section—multiple cell model, assuming that the tissue is homogeneous (mathematically, the measured values of a feature are dense and continuous).

One sees that the sum of the squares of pooled data is the sum of the squares of variability between the cells and the squares of variability between the sections (see Appendix 2). Therefore, to test the significance of the difference between two groups of cells by Student's t test, we can use the standard deviation of the pooled data in lieu of the standard deviation among the cells whose sample size is M without violating the critical region regardless of the magnitude of the number of sections. We use $m = 1$ for a computation.

Using the same process as shown in the multiple section—single cell model, and from the principle discussed immediately above, one sees in the single section—multiple cell model that

$$\bar{R} = \frac{2}{\pi} \bar{L}, \tag{14}$$

$$\bar{A} = \frac{4}{\pi} \bar{L}, \tag{15}$$

$$\bar{r} = \frac{2}{\pi} \bar{l}^*, \tag{16}$$

and

$$\bar{a} = \frac{4}{\pi} \bar{l}^{*2}. \tag{17}$$

$\bar{R}$, $\bar{A}$, $\bar{r}$, and $\bar{a}$ are the estimators of $\hat{R}$, $\hat{A}$, $\hat{r}$, and $\hat{a}$.

The standard errors, $\Delta\bar{R}$, $\Delta\bar{A}$, $\Delta\bar{r}$, and $\Delta\bar{a}$ are:

$$\Delta\bar{R} = \frac{2}{\pi} \Delta\bar{L}, \tag{18}$$

$$\Delta\bar{A} = \frac{8}{\pi} \bar{L} \cdot \Delta\bar{L}, \tag{19}$$

$$\Delta\bar{r} = \frac{2}{\pi} \Delta\bar{l}^*, \tag{20}$$

and

$$\Delta\bar{a} = \frac{8}{\pi} \bar{l}^* \cdot \Delta\bar{l}^*. \tag{21}$$

In a derivation similar to that of Eq. 13, the mean number of pseudopodia per cell $\bar{N}$, and its standard error $\Delta\bar{N}$ are calculated as follows:

$$\bar{N} = \frac{1}{M} \sum_i^M \bar{N}_i, \tag{22}$$

$$\Delta N = \frac{1}{M} \sqrt{\sum_i^M \bar{N}_i^2 - M\bar{N}^2}, \tag{23}$$

where

$$\bar{N}_i = \bar{n}_i \frac{\bar{L}_i}{\bar{l}_i}.$$

The standard deviation is $\Delta N \cdot \sqrt{M}$.

The ratio of the sum of the cross-sectional areas of the pseudopodia and the base area of the ith basal cell,

$$\bar{F}_i = \frac{\sum_k^{\bar{n}_i} \bar{l}_{ik}}{\bar{L}_i} = \bar{n}_i \frac{\bar{l}_i}{\bar{L}_i}.$$

The mean of $\bar{F}_i$ between the cells,

$$\bar{F} = \frac{1}{M} \cdot \sum_i^M \bar{F}_i. \tag{24}$$

[1] One does not need to assume that the cross sections of the cells and pseudopodia are circular for validation of Eq. 11.

[2] Expanding $\bar{N}_i = (\hat{n}_i + \Delta\hat{n}_i + \Delta\hat{n}_i) \cdot (\hat{l}_i + \Delta\hat{l}_i)/(\hat{L}_i + \Delta\hat{L}_i)$ around $\hat{N}_i$, one sees that $\bar{N}_i \to \hat{N}_i$ as $i \to \infty$

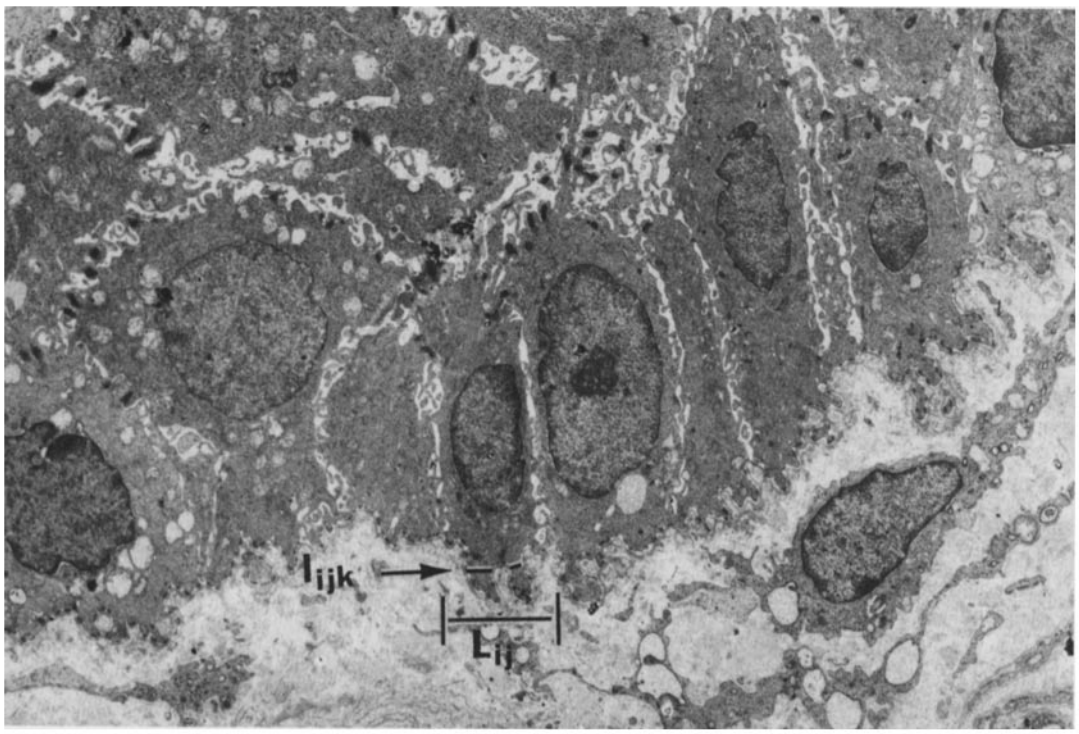

FIGURE 4 An electron micrograph of the basal cells of normal human uterine cervix, demonstrating actual measurement of L_{ij} and l_{ijk}. ×4,500.

The standard error of $\bar{F}$,

$$\Delta\bar{F} = \frac{1}{M} \cdot \sqrt{\sum_{i}^{M} \bar{F}_i^2 - M\bar{F}^2}. \qquad (25)$$

The standard deviation of $\bar{F}_i$ is $\Delta\bar{F} \cdot \sqrt{M}$.

MATERIALS AND METHODS

The human uterine cervical tissues were obtained by colposcope-directed biopsies using the Kevorkian forceps. We used specimens obtained from three patients of each category of lesions, i.e., reactive atypia, mild dysplasia, and controls (normal epithelium). The specimens were immediately placed in a phosphate-buffered 1% glutaraldehyde, 4% formalin solution described by McDowell et al (6). The specimens were dehydrated and embedded in paraffin in the usual manner. 5- to 7-μm thick sections were stained with hematoxylin and eosin and examined under a light microscope. After confirming that the desired cervical squamous epithelial area was located in the paraffin block, we excised cubes of ~0.5 × 0.5 × 0.5 mm from the paraffin blocks. The samples were deparaffinized and rehydrated by passing them through a descending series of aqueous ethanol solutions. The samples were osmicated, dehydrated through ethanol, and embedded in Epon 812 for examination by transmission electron microscopy. 500-nm Epon sections were stained with a 1% methylene blue, 1% Azure B solution and examined to ensure that the epithelial-stromal interface was in the block and that the section orientations were not tangential to the basal lamina. 70- to 100-nm thin sections were mounted on Formvar-coated copper grids, poststained with lead citrate and uranyl acetate, and examined in a modified JEOL 100B electron microscope in the transmission microscope mode at 60 kV of accelerating voltage.

The electron micrographs of the epithelial-stromal interface taken at approximate magnifications of 5,000 were printed on 8″ × 10″ Kodak photographic paper. Between the specimen observations, the actual magnifications were repeatedly calibrated using a carbon grating replica (E. F. Fullam, Inc., N. Y.) with 2160 lines/mm. The final magnifications of the prints were calculated from the original magnifications of the electron micrographs and enlarging factors of the prints. The length of the intersect of the section plane with the base of the basal cells (L_{ij}) and the length of the intersect of the section plane with the base of the pseudopodia (l_{ijk}) were measured with a ruler, and the number of pseudopodia (n_{ij}) was counted as shown in Fig. 4 (note that $\bar{L}_i, \bar{l}_{ik}$, are means of L_{ij}, l_{ijk}, and n_{kj} for $m = 1$). The values of $\bar{L}_i$'s and $\bar{l}_{ik}$'s were converted to the original sizes, dividing the observed sizes on the prints by the magnification factors. The means $\bar{L}$, $\bar{l}^*$ and their standard errors were computed. The mean $\bar{N}$ and its standard error were calculated by Eqs. (22) and (23); and the ratio $\bar{F}$ and its standard error were calculated by Eqs. (24) and (25) using a Digital Equipment Corporation PDP/8F computer.[3] The manual calculation shown in Table I is an example of the actual process translated into the computer program.

RESULTS

The mean radius and diameter of the normal epithelial basal cells were 2.70 μm ± 0.116 (standard error) and 5.40 μm ± 0.232 (standard error), respectively. The mean radius and diameter of pseudopodia were 0.287 μm ± 0.011 (standard error) and 0.573 μm ± 0.023 (standard error), respectively. Calculating from these values, the mean base area of the normal epithelial basal cell was 22.9 μm^2 ± 1.97 (standard error), and the mean base area of the pseudopodia of normal epithelial basal cells was 0.258 μm^2 ± 0.021 (standard error). Using Eqs. (22), (23), (24), and (25), the number of the pseudopodia per cell, $\bar{N}$, and the ratio of the total base area of the pseudopodia to the base area of the basal cell, $\bar{F}$, were 34.32 ± 2.92 (standard error) and 0.338 ± 0.018 (standard error), respectively. The results are summarized in Table II.

Measurements of the specimens defined as reactive atypia and mild dysplasia were obtained in the same way. The values of $\bar{N}$ and $\bar{F}$ on these two pathological conditions and controls are shown in Table III. Reactive atypia and mild dysplasia demonstrated statistically significant reductions of the number of pseudopodia per cell ($\bar{N}$) and the ratio of total base areas ($\bar{F}$) when compared to the control normal cervical epithelium.

DISCUSSION

Intercellular communication regulating cell proliferation and differentiation is believed to occur between cells through cer-

[3] The source program was written in ANSI FORTRAN IV for DEC PDP 8/F computer. A copy of the source program is available from the first author upon request.

TABLE I

The observed values of L_{ij}, l_{ijk}, $\bar{l}_i$, and $\bar{n}_i$.

Sequential number of basal cell	Length of intersect L_{ij} (μm)	Length of intersect l_{ijk} (μm)	Mean of l_{ijk} ($\bar{l}_i$)	Number of pseudopodia in the section n_{ij}	Total number of pseudopodia per cell $\bar{N}_i = \bar{n}_i \cdot \bar{L}_i / \bar{l}_i$	The ratio of the total area of pseudopodia to basal area of basal cell $\bar{F}_i = \bar{n}_i \cdot \bar{l}_i / \bar{L}_i$
1	5.0542	0.4813	0.5616	3	27.00	0.333
		0.3610				
		0.8424				
2	4.2118	0.4813	0.5415	2	15.56	0.257
		0.6017				
3	4.8135	0.1805	0.3312	4	58.19	0.275
		0.3018				
		0.4813				
		0.3610				
⋮	⋮	⋮	⋮	⋮	⋮	⋮
⋮	⋮	⋮	⋮	⋮	⋮	⋮
56	4.5989	0.3209	0.2781	5	82.69	0.302
		0.4278				
		0.2139				
		0.1070				
		0.3209				
Total Observations	56	180	56	56	56	56
Mean ± S.E.	$\bar{L} = 4.240$	$\bar{l}^* = 0.4534$	$\bar{l} = 0.4530$	$\bar{n} = 3.214$	$\bar{N} = 34.317$	$\bar{F} = 0.338$
	± 0.182	± 0.0242	± 0.0200	± 0.176	± 2.922	± 0.018

From the means and the standard errors, $\bar{L}$, $\bar{l}$, $\Delta\bar{L}$, and $\Delta\bar{l}$, other values shown in Table II were computed using Eqs. 22, 23, 24 and 25.

TABLE II

Calculated values of radius ($\bar{R}$), diameter ($\bar{D}$), base areas ($\bar{A}$) of the basal cell; radius ($\bar{r}$), diameter ($\bar{d}$), area ($\bar{a}$) of the pseudopodia, the number of pseudopodia per cell ($\bar{N}$) and the ratio of total base areas of pseudopodia to base area of basal cell ($\bar{F}$) in normal cervical epithelium.

Basal cell			Pseudopodium			Number of pseudopodia per cell ($\bar{N}$)	Ratio of areas ($\bar{F}$)
radius ($\bar{R}$)	diameter ($\bar{D}$)	area ($\bar{A}$)	radius ($\bar{r}$)	diameter ($\bar{d}$)	area ($\bar{a}$)		
2.70 μm	5.40 μm	22.9 μm^2	0.287 μm	0.573 μm	0.258 μm^2	34.32	0.338
(±0.116)	(±0.232)	(±1.97)	(±0.011)	(±0.023)	(±0.021)	(±2.92)	(±0.018)

The calculations were made using Eqs. 22, 23, 24 and 25.
Standard errors are shown in the parenthesis.
$\bar{L}$: 4.240 μm ±0.182 (S.E.), $\bar{l}^*$: 0.453 μm ±0.024 (S.E.), $\bar{n}$: 3.214 ± 0.176 (S.E.).

tain morphological structures that can be identified in electron microscopic studies of cellular membranes in squamous epithelium. These structures can be categorized as gap junctions, desmosomes, and pseudopodia. The precise function of these individual organelles is not fully elucidated. Various authors have noted a decrease in gap junctions in neoplastic alterations of epithelial cells or in premalignant conditions (dysplasia or carcinoma in situ) of the squamous epithelium of the human uterine cervix (10).

Shingleton et al. reported that the number of pseudopodia was reduced qualitatively in the basal cells of advanced premalignant conditions of the uterine cervical squamous epithelium designated as severe dysplasia and carcinoma in situ (10). These qualitative differences were noted during visual observation with the transmission electron micrographs. Our newly developed highly sensitive morphometric method enabled us to detect quantitative reductions in the number of pseudopodia in reactive atypia, abnormality associated with underlying inflammation, and in mild dysplasia, the earliest form of premalignant condition of the uterine cervical squamous epithelium. It remains to be seen, however, whether the reduction of pseudopodia is a phenomenon that is analogous and related to the reported reduction of other intercellular communication structures such as the gap junction and desmosome in neoplastic tissues[3, 7, 8] (see Addendum).

The calculation of expectancy in Eq. 1 shows that the actual diameter of an object proves to be $\frac{4}{\pi}$ of the mean value of the measured diameter on a section plane. Thus, the mean of the intersects of a section plane with two-dimensional objects is smaller than the actual mean diameter of the objects. Such misleading information on the mean diameter of circular objects was shown in the previous publication (5) and the discrepancy is sometimes erroneously attributed to the shrinkage of the tissue due to fixation. As stated in the footnote, Eq. 11 does not need to assume that the base of a pseudopodium or a basal cell is circular. There are, however, certain mathematical constraints on the shape for this method to be correctly applied. We did not use the correction for errors due to section thickness demonstrated by Weibel et al. (Holms' correction) for $\bar{L}$, $\bar{l}$ and $\bar{l}^*$ (11). This omission will cause systemic errors in our calculations of $\bar{N}$ or $\bar{F}$. Nevertheless, in all specimens used, the demonstrated reductions of $\bar{N}$ and $\bar{F}$ of the epithelial cells in pathological conditions are valid, as the section thickness is constant.

TABLE III

The number of pseudopodia per cell ($\bar{N}$) and the ratio of total base areas of pseudopodia to base area of basal cell ($\bar{F}$) obtained from normal cervical epithelium, reactive atypia and mild dysplasia of cervical epithelium.

	Normal cervical epithelium	Reactive atypia	Mild dysplasia
Mean number of pseudopodia ($\bar{N}$)	34.32 ± 2.92	23.62 ± 4.39	26.98 ± 4.13
Probability of t test on the difference compared to normal	—	0.025 > p	0.1 > p
Ratio of the base area of pseudopodia and that of the cell ($\bar{F}$)	0.338 ± 0.018	0.188 ± 0.026	0.226 ± 0.022
Probability of t test on the difference compared to normal	—	0.001 > p	0.001 > p

APPENDIX 1

We used the following symbols in the mathematical equations. A schematic illustration of the representative variables is shown in Fig. 5.

$\hat{A}_i$: The expectancy of the base area of the ith basal cell ($i = 1, \ldots, M$).

$\bar{A}_i$: The base area of the ith basal cell calculated from $\bar{L}_i$.

$\hat{A}$: The mean of $\hat{A}_i$ in terms of i.

$\bar{A}$: The base area of the basal cells calculated from $\bar{L}$.

$\hat{a}_{ik}$: The expectancy of the base area of the kth pseudopodium ($k = 1, \ldots, \hat{n}_i$) of the ith cell ($i = 1, \ldots, M$).

$\hat{a}_i$: The expectancy of the base area of the ith cell calculated from $\hat{l}_i$.

$\bar{a}_i$: The base area of the pseudopodium of the ith cell calculated from $\bar{l}_i$.

$\hat{a}$: The mean of $\hat{a}_i$ in terms of i.

$\bar{a}$: The base area of the pseudopodia calculated from $\bar{l}^*$.

$\hat{F}_i$: The expectancy of the ratio of the total area of pseudopodia and the area of the base of the ith basal cell.

$\bar{F}_i$: The observed ratio of the total area of pseudopodia and the area of the base of the ith basal cell.

$\bar{F}$: The mean of $\bar{F}_i$ in terms of i.

L_{ij}: The observed value of the length of the intersect of the base of the ith cell with the jth section plane ($j = 1, \ldots, m$).

$\hat{L}_i$: The expectancy of the length of the intersect of the base of the ith basal cell with a section plane.

$\bar{L}_i$: The mean of L_{ij} in terms of j.

$\hat{L}$: The mean of $\hat{L}_i$ in terms of i.

$\bar{L}$: The mean of $\bar{L}_i$ in terms of i.

l_{ijk}: The observed length of the intersect of the base of the kth pseudopodium of the ith cell observed in the jth section plane.

$\hat{l}_{ik}$: The expectancy of the length of the intersect of the base of the kth pseudopodium of the ith cell.

$\bar{l}_{ik}$: The mean of l_{ijk} in terms of j for $l_{ijk} \neq 0$

$\bar{l}_{ij}$: The mean of l_{ijk} in terms of k for $l_{ijk} \neq 0$

$\hat{l}_i$: The expectancy of the length of the intersect of the base of a pseudopodium of the ith cell. Note that

$$\hat{l}_i \neq \frac{1}{\hat{N}_i} \sum_k^{\hat{N}_i} \hat{l}_{ik}.\|$$

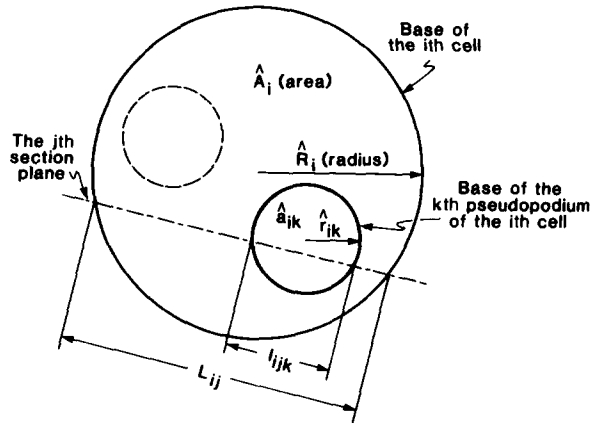

FIGURE 5 Schematic representation of the bottom view of a basal cell illustrating mathematical symbols.

$\bar{l}_i$: The mean of $\bar{l}_{ij}$ in terms of j for $\bar{l}_{ij} \neq 0$, or, the mean of $\bar{l}_{ik}$ in terms of k.

$\hat{l}$: The mean of $\hat{l}_i$ in terms of i.

$\bar{l}$: The mean of $\bar{l}_i$ in terms of i.

$\bar{l}^*$: The pooled mean of $\bar{l}_{ik}$ in terms of i and k, i.e.,

$$\frac{1}{\sum_i^M \bar{n}_i} \sum_i^M \sum_k^{\bar{n}_i} \bar{l}_{ik},$$

i.e., weighted mean of $\bar{l}_i$ in terms of i.

N_{ij}: The total number of the pseudopodia in the ith cell calculated from n_{ij}, $\bar{l}_{ij}$, and $\bar{L}_{ij}$.

$\hat{N}_i$: The expectancy of the number of the pseudopodia of the ith cell.

$\bar{N}_i$: The mean of N_{ij} in terms of j.

$\hat{N}$: The mean of $\hat{N}_i$ in terms of i.

$\bar{N}$: The mean of $\bar{N}_i$ in terms of i.

‖ The chance that a single randomly placed section plane falls on the kth pseudopodium is

$$\frac{\hat{a}_{ik}}{\hat{A}_i} = \frac{\hat{l}_{ij}^2}{\hat{L}_i^2}.$$

The expectancy of the length of the intersect is $\hat{l}_{ik}$. Hence, the expectancy of the length of the intersect with any pseudopodium is

$$\hat{l}_i = \frac{\sum_k^{\hat{N}_i} \frac{\hat{l}_{ik}^3}{\hat{L}_i^2}}{\sum_k^{\hat{N}_i} \frac{\hat{l}_{ik}^2}{\hat{L}_i^2}} = \frac{\sum_k^{\hat{N}_i} \hat{l}_{ik}^3}{\sum_k^{\hat{N}_i} \hat{l}_{ik}^2}.$$

Whereas, the mean of the expectancies of the intersects on the first through the $\hat{N}_i$th pseudopodia is

$$\hat{\hat{l}}_i = \frac{1}{\hat{N}_i} \sum_k^{\hat{N}_i} \hat{l}_{ik}.$$

The latter is not equal to $\hat{l}_i$. To approximate $\hat{\hat{l}}_i$ with $\hat{l}_i$, the second and the third moments of $\hat{l}_{ik}$ must be small.

n_{ij}: The number of pseudopodia observed in the ith cell in the jth section plane.
$\hat{n}_i$: The expectancy of the number of pseudopodia observed in the ith cell in a section plane.
$\bar{n}_i$: The mean of n_{ij} in terms of j.
$\bar{n}$: The mean of $\bar{n}_i$ in terms of i.
$\hat{R}_i$: The radius of the circular base of the ith basal cell.
$\bar{R}_i$: The radius of the circular base of the ith cell calculated from $\bar{L}_i$.
$\hat{R}$: The mean of $\hat{R}_i$ in terms of i.
$\bar{R}$: The radius of the bases of the basal cells calculated from $\bar{L}$.
$\hat{r}_{ik}$: The radius of the circular base of the kth pseudopodium of the ith cell.
$\hat{r}$: The radius of circular base of the pseudopodium calculated from $\hat{l}$.
$\bar{r}_i$: The radius of the circular base of the pseudopodium of the ith cell calculated from $\bar{l}_i$.
$\bar{r}$: The radius of the circular base of the pseudopodium calculated from $\bar{l}$*.

APPENDIX 2

To generalize the discussion, let x_{ij} be a measure of a feature of the ith cell on the ith section plane, let $\hat{x}_i$ be an expectancy of the measure of the ith cell, and let $\bar{x}_i$ be the estimator of $\hat{x}_i$ after observations of finite m section planes. Let $\bar{x}$ be the mean of $\bar{x}_i$'s after observing a sample of M cells, $\hat{x}$ be the mean of $\hat{x}_i$'s ($\hat{x}$ should not be confused with the population mean). That is,

$$\bar{x}_i = \frac{1}{m}\sum_{j}^{m} x_{ij}, \tag{A1}$$

$$\bar{x} = \frac{1}{M}\sum_{i}^{M} \bar{x}_i, \tag{A2}$$

and

$$\hat{x} = \frac{1}{M}\sum_{i}^{M} \hat{x}_i. \tag{A3}$$

Let us assume that the distribution function of x_{ij} in terms of j is not Gaussian as in the model shown in Fig. 2. We can assume from the model in Fig. 2 that the distribution of x_{ij} in terms of j will be identical if $\hat{x}_i$'s are identical. Inasmuch as we can assume that a subset of the cell population that has the identical $\hat{x}_i$'s, say $\hat{x}_c$, contains a large number of samples, the mean of $\bar{x}_i$'s (the estimators of the means of x_{ij}'s for j) in such subset is distributed around $\hat{x}_c$ in a Gaussian distribution and converges to $\hat{x}_c$ by the central-limit theorem.¶

Thus, $\bar{x}$, the mean of all $\bar{x}_i$'s, is the weighted mean of the means having Gaussian distribution. Further, we can say that $\bar{x}$ converges to $\hat{x}$, the mean of $\hat{x}_i$'s, if the sample size is sufficiently large. Let the standard deviation of $\bar{x}_i$ be s.

We need an estimator of the variance between the cells defined by

$$Ms^2 = \sum_{i}^{M} (\bar{x}_i - \bar{x})^2. \tag{A4}$$

¶ Mathematically the following conditions are necessary:
(*A*) $\hat{x}_i$'s are dense, that is, a sufficiently large number of $\hat{x}_i$'s are present within an interval between $\hat{x}_c$ and $\hat{x}_c + \Delta\hat{x}_c$ for a small $\Delta\hat{x}_c$.
(*B*) The distribution function of $\hat{x}_i$'s is identical for all $\hat{x}_i$'s within the interval $\hat{x}_c$ and $\hat{x}_c + \Delta\hat{x}_c$ for any $\hat{x}_c$.

First, we obtain the sum of squares of the pooled data after an observation of m section planes of M cells. Let s' be the standard deviation of the pooled data such that

$$\begin{aligned} mMs'^2 &= \sum_{i}^{M}\sum_{j}^{m} (x_{ij} - \bar{x})^2 = \sum_{i}^{M}\sum_{j}^{m} \{(x_{ij} - \bar{x}_i) + (\bar{x}_i - \bar{x})\}^2 \\ &= \sum_{i}^{M}\sum_{j}^{m} (x_{ij} - \bar{x}_i)^2 + 2\sum_{i}^{M}\sum_{j}^{m} \{(x_{ij} - \bar{x}_i)(\bar{x}_i - \bar{x})\} \\ &\quad + \sum_{i}^{M}\sum_{j}^{m} (\bar{x}_i - \bar{x})^2 \\ &= \sum_{i}^{M}\sum_{j}^{m} (x_{ij} - \bar{x}_i)^2 + m\sum_{i}^{M} (\bar{x}_i - \bar{x})^2. \end{aligned} \tag{A5}$$

Hence,

$$Ms'^2 > Ms^2. \tag{A6}$$

It also follows that the degree of freedom in a statistical test of significance is to be calculated from the number of the cells observed, M; not from the number of pseudopodia observed. For instance, assume that an observation on M cells is compared to another on M' cells by Student's t test, the degree of freedom is $M + M' - 2$.

Expanding the above discussion further, one sees that observation on more than one section through the same cell can be treated as if different cells are observed. For instance, when m section planes of M cells are observed, the data can be treated as if $M \cdot m$ cells were observed by single section—multiple cell model. In practice, more than one microtome section can be made from one block; yet one does not need to worry whether some of the cells are redundantly observed.

The authors wish to thank Jean Engbring and Joan Wuertz Fredson for their technical assistance in electron microscopic tissue preparation, and Lisa Budenski for typing the manuscript.

Received for publication 15 April 1981, and in revised form 20 July 1981.

ADDENDUM

After the manuscript was submitted for publication, two reports of morphometric analyses of the number of desmosomes and the numbers of gap junctions in dysplasia and carcinoma *in situ* of the uterine cervical epithelium appeared:

Lawrence, W. D., S. M. Shingleton, H. Goore, and S. J. Soong. 1980. Ultrastructural and morphometric study of diethylstilbesterol-associated lesions diagnosed as cervical intraepithelial neoplasia III. *Cancer Res.* 40:1558–1567.

Koch, O., M. Amandruz, A. M. Shindler, and G. Gabiani. 1981. Desmosomes and gap junctions in precarcinomatous and carcinomatous conditions of squamous epithelia. An electron microscopic and morphometrical study. *J. Submicrosc. Cytol.* 2:267–281.

REFERENCES

1. Cooper, M., and H. Pinkus. 1977. Intrauterine transplantation of rat basal cell carcinoma as a model for reconversion of malignant to benign growth. *Cancer Res.* 37:2544–2552.
2. Cunha, G. R., B. Lung, and B. Reese. 1980. Glandular epithelial induction by embryonic mesenchyme in adult epithelium of BALB/B mice. *Invest. Urol.* 17:302–304.
3. Elias, P. M., S. Grayson, T. M. Caldwell, and N. S. McNutt. 1980. Gap junction proliferation in retinoic acid-treated human basal cell carcinoma. *Lab. Invest.* 42:469–475.
4. Daw, G. J. 1972. Epithelial-mesenchyme interactions in relation to the genesis of polypma virus-induced tumors of mouse salivary glands. *In* Tissue Interactions in Carcinogenesis. D. Tarin, editor. Academic Press, Inc., New York. 305–358.
5. Loud, A. V. 1974. Sterological determination of nuclear pore density from thin sections of

nuclear membrane. *Proc. E.M.S.A.* 274–275.
6. McDowell, E. M., and B. J. Trump. 1976. Histologic fixative suitable for diagnostic light and electron microscopy. *Arch. Pathol. Lab. Med.* 100:405–414.
7. McNutt, N. S., and R. S. Weinstein. 1969. Carcinoma of the cervix: deficiency of nexus intercellular junctions. *Science (Wash. D. C.)* 165:597–599.
8. Nicolson, G. L., and G. Poste. 1976. The cancer cell: dynamic aspects and modifications in cell surface organization. *N. Engl. J. Med.* 295:197–203, 253–258.
9. Sakakura, T., Y. Sakagami, and Y. Nishizuka. 1979. Acceleration of mammary cancer development by grafting of fetal mammary mesenchymes in C3H mice. *Gann.* 70:459–466.
10. Shingleton, H. M., R. M. Richart, J. Weiner, and D. Spiro. 1968. Human cervical intraepithelial neoplasia: fine structure of dysplasia and carcinoma in situ. *Cancer Res.* 28: 695–706.
11. Weibel, E. R., and D. Paumgartner. 1978. Integrated stereological and biochemical studies on hepatocytic membranes. II. Correlation of section thickness on volume and surface density estimates. *J. Cell Biol.* 77:584–597.